



RESEARCH ARTICLE

10.1029/2018RS006727

Ionospheric Plasma Bubble Zonal Drift Derived From Total Electron Content Measurements

R. P. Silva^{1,2} , J. R. Souza¹ , J. H. A. Sobral¹ , C. M. Denardini¹ , G. L. Borba³ , and M. A. F. Santos² ¹Instituto Nacional de Pesquisas Espaciais, São José dos Campos, São Paulo, Brazil, ²Centro Regional do Nordeste (CRN/INPE), Natal, Brazil, ³Departamento de Geofísica, Universidade Federal do Rio Grande do Norte, Natal, Brazil

Key Points:

- Automatic calculation of the plasma bubbles velocities by LTIAM model
- Using GNSS signals to infer plasma bubbles velocities

Correspondence to:

R. P. Silva,
regiapereira@gmail.com;
regia.pereira@inpe.br

Citation:

Silva, R. P., Souza, J. R., Sobral, J. H. A., Denardini, C. M., Borba, G. L., & Santos, M. A. F. (2019). Ionospheric plasma bubble zonal drift derived from total electron content measurements. *Radio Science*, 54, 580–589. <https://doi.org/10.1029/2018RS006727>

Received 14 SEP 2018

Accepted 16 MAY 2019

Accepted article online 3 JUN 2019

Published online 18 JUL 2019

Abstract Equatorial plasma bubbles consist of field-aligned large-scale depletions, or irregularities, characterized by drastic ion density rarefactions of the nocturnal low latitude/equatorial ionosphere. Understanding their behavior is important because of their degrading effects on radio wave signals and, consequently, their respective technological applications such as, for example, Global Positioning System applications. In this sense, a methodology of pattern recognition was developed and implemented here using the Long-Term Ionospheric Anomaly Monitoring in order to infer the plasma bubbles zonal drift velocities, using two receiving stations of global navigation satellite systems data from the Brazilian Continuous Monitoring Network, located near to each other, in Salvador (BA) during geomagnetically quiet periods. The study covered the years of 2012, 2013, and 2014 for the months from September to January of the following year, choosing 10 representative days for each month. The average results for the plasma bubble zonal velocities provided by the model calculations were in agreement with the well-known values. However, monthly individual analysis showed a behavior anticorrelated with that expected for high solar flux. Probably, the unexpected behavior is due to atypical configuration of the solar activity ascending phase.

1. Introduction

Equatorial plasma bubbles (EPBs) are large-scale depletions that occur in the equatorial ionospheric plasma density. The eastward electric field generated by the ionospheric *E* region dynamo during the day causes the *F* region vertical up drift $\mathbf{E} \times \mathbf{B}$. After sunset the ionization due to solar radiation decreases in the *E* region, causing the domain of the *F* region dynamo. Due to this dynamo, there is an increase in the eastward electric field just after sunset, and as a consequence, the ionospheric plasma moves to higher altitudes, where the ionic collisional frequency with neutral particles decreases significantly. This fact favors development of ionospheric plasma bubbles through the by Rayleigh-Taylor instability mechanism because the growth rate is inversely proportional to the collisional frequency (Abdu, 2001; Huang & Kelley, 1996; Kelley, 2009). Figure 1 presents a time sequence with arise and development of EPBs observed by optical technique operating in the 630 nm for the atomic oxygen luminescence. The airglow observations were obtained in Sao Joao do Cariri, Brazil (7°S, 36°W) during the night of 15 November 2012. The plasma bubble is seen forming a dark structure from the first left top panel, moving to eastward and developing multiple structures and bifurcations. The EPBs also have small internal structures of the order of centimeters to tens of kilometers. Thus, the EPBs can interfere in transionospheric telecommunication signals and related applications (Moraes et al., 2018).

The plasma bubbles have been extensively monitored by optical techniques (Haase et al., 2011; Sobral, Abdu, & Batista, 1980; Sobral, Abdu, Zamlutti, et al., 1980), Digisondes (Abdu, 2001; Abdu et al., 1983), radio scintillations (Aarons, 1993), rocket soundings (Abdu et al., 1991; LaBelle et al., 1997), and satellites (Burke et al., 2004; Huang et al., 2002; Moraes et al., 2018; de Rezende et al., 2007). Besides that, several theoretical and numerical studies (Haerendel et al., 1992; Huba & Joyce, 2010; Sousasantos et al., 2017) have been performed to investigate EPB generation mechanism and dynamics. In this perspective, the LTIAM (Long-Term Ionospheric Anomaly Monitoring) was developed to identify and calculate the ionospheric delay gradients resulting from the passage of the ionospheric irregularities (Jung & Lee, 2012). It is well known that ionospheric irregularities may represent a threat to the adequate use of global navigation satellite systems (GNSS) in the air navigation, and consequently, do not ensure the safety and integrity of users of these systems. Initially, the LTIAM was developed to support the use and evaluate the limitations of augmentation systems of Global Positioning System to identify the effects of the ionosphere on the air traffic control

©2019. The Authors.

This is an open access article under the terms of the Creative Commons Attribution-NonCommercial-NoDerivs License, which permits use and distribution in any medium, provided the original work is properly cited, the use is non-commercial and no modifications or adaptations are made.

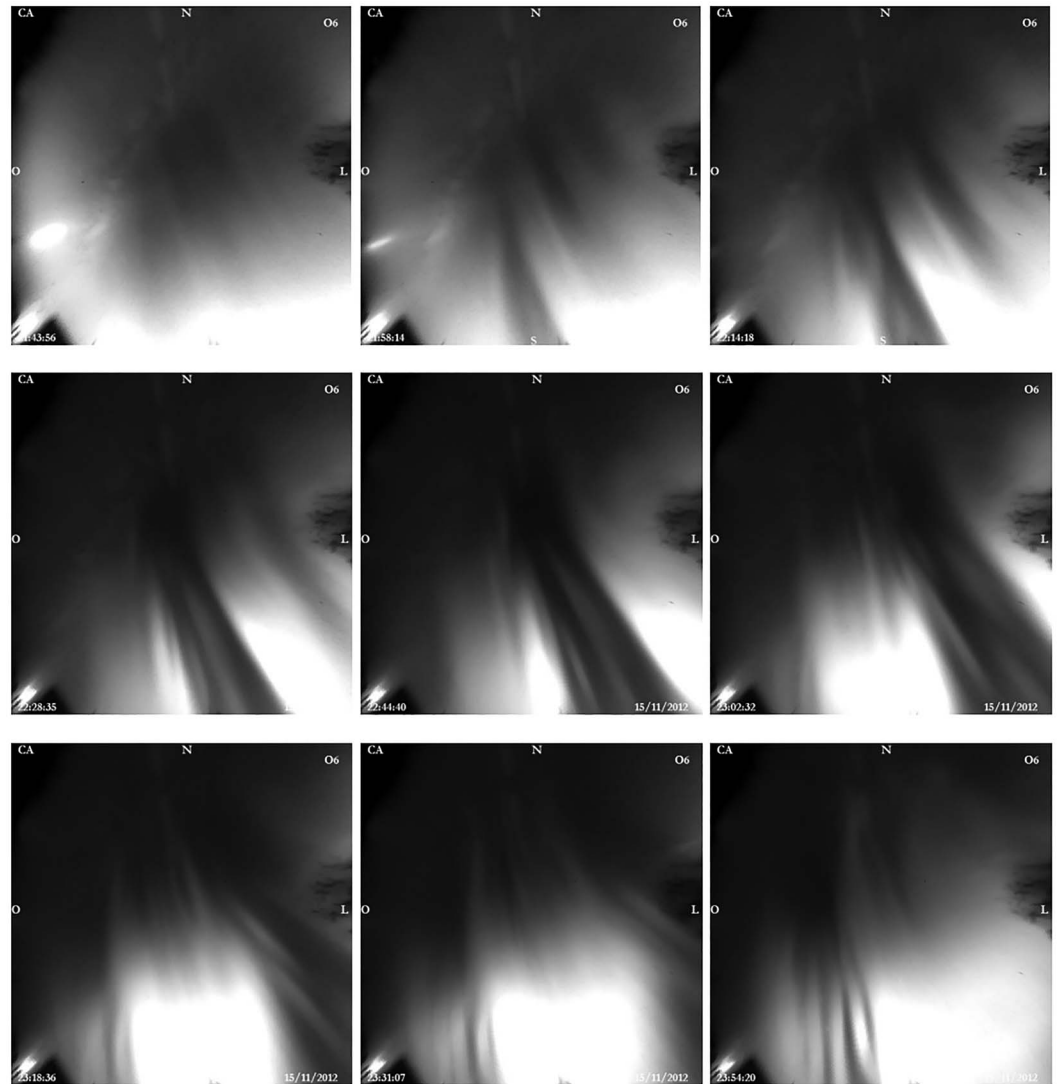


Figure 1. Sequence of the OI 630-nm airglow observations obtained in Sao Joao do Cariri, Brazil, during the night of 15 November 2012, from 21:43:66 to 23:54:20 UT. The bubble is seen from the first left top panel, evolving to the eastward and developing multiple structures and bifurcations. The images were treated and the stars removed.

and, essentially, in the prevention of accidents during aircraft takeoff and landing (Lee et al., 2011; Pullen et al., 2009; Takeyasu et al., 2009). In this work, the LTIAM was used to automatically monitor the ionospheric irregularities, and from it to infer the EPB zonal drift velocities by using simultaneous data from two GNSS receiving stations closely located to each other. For this purpose we use a procedure called Station Pair Method or Two Station Method, where each selected station records the passage of the irregularity, and from that record a pattern recognition algorithm, *k*-means, is used.

2. Data and Methodology

As mentioned before, in this study, the LTIAM was used to monitor the EPBs in order to infer the zonal drift velocities from GNSS data. In the following sections the data and methodology will be presented.

2.1. Data

In this paper we have used data of two GNSS receiving stations by Brazilian Continuous Monitoring Network – RBMC (<https://ww2.ibge.gov.br/home/geociencias/geodesia/rbmc/rbmc.shtm?c=7>). Both stations chosen for this study are located in Salvador, Brazil. Figure 2 shows a map with the stations' positions



Figure 2. South America map (left panel) showing the stations' position used in the present study. Both stations are localized Salvador, Brazil, and are designed by SSA1 and SAVO.

and respective coordinates. The stations are designed by SSA1 and SAVO. The magnetic coordinates were obtained from the International Geomagnetic Reference Field, taking into account 350 km of altitude for the year of 2013.

Sobral et al. (2002) verified that the highest occurrence rate of plasma bubbles during high solar activity over the Brazilian region occurs during the months of September to April. To ensure the coverage of representative data, this study covered the years of 2012, 2013, and 2014 from September until January of the following year, using 10 days as representative of each month, all with occurrence of plasma bubbles duly verified by OI 6,300-nm airglow images. Since the EPB occurrence is uncommon during low solar activity, the data were selected for $F10.7 \geq 130 \cdot 10^{-22} \cdot \text{Wm}^{-2} \cdot \text{Hz}^{-1}$. In order to minimize the effects of the geomagnetic storms, it was considered only the data for the days which $\Sigma Kp \leq 24$. Figure 3 shows the levels of F10.7 and ΣKp for the days of our study. The years chosen for this study represent ascendant phase and maximum solar cycle 24. The left top panel corresponds to the year 2012, while the right top panel corresponds to 2013. The bottom panel refers to 2014. The data represented in bars refer to F10.7 values in the left-hand ordinate, while the data in scatter represent the ΣKp values in the right-hand ordinate. The hatched areas in the 2012 and 2013 panels represent a gap in the database. It does not mean there were no plasma bubble events in these months; it just means that the EPB event days did not fill the requirements established in this study. Likewise, this study does not cover the months from February to April due to both the F10.7 minimum value established in this study and the availability of GNSS data simultaneously during occurrences of EPBs in the referred months.

2.2. Methodology

The LTIAM was developed by the Korean Advanced Institute of Science and Technology and Tetra Tech AMT as a monitoring tool of Ground-Based Augmentation Systems. The LTIAM process RINEX files remove the bias; check the potential occurrence of an ionospheric storm on a given day, based on space weather indices; and calculate the ionospheric delays.

In this work, it was used a methodology called *Two Station Method* (Bang & Lee, 2013; Datta-Barua et al., 2010; Jung & Lee, 2012) to study the ionospheric delays caused by EPBs. Assuming that the delay for each station i and j , seen by the same satellite, is different, the ionospheric delay (d) is estimated by dividing the difference between the signal time delays between each receiver (I) and the satellite (k) by the distance between the receivers:

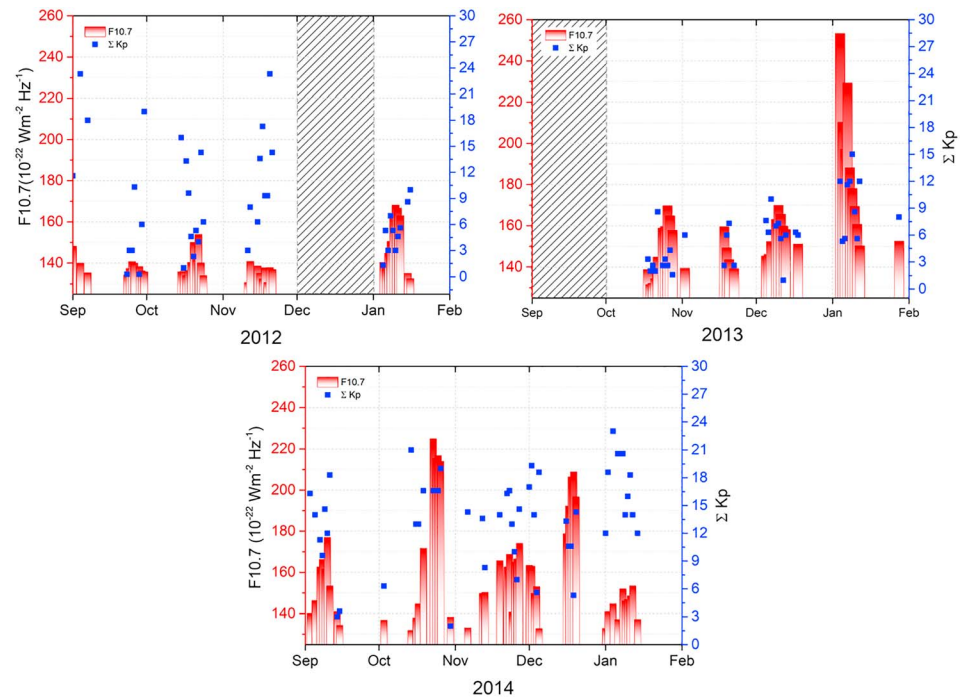


Figure 3. Database classification regarding the Kp index and solar flux. The data in bars refer to F10.7 values (left-hand ordinate), while the scatter chart data the ΣKp values (right-hand ordinate). The top panels correspond to the years 2012 (left) and 2013 (right), and the bottom panel refers to 2014. The hatched areas in 2012 and 2013 panels represent a gap in the database.

$$d = \frac{|I_i^k(t) - I_j^k(t)|}{\|x_i - x_j\|}$$

where x_i and x_j are the locations of i and j stations, respectively, and I is the slant total electron content. The top panel in Figure 4 illustrates the Two Station Method. In the illustration, the EPB is represented by the blue (time 1) and red (time 2) curves. When a plasma bubble occurs, both GNSS receiving stations record the irregularity. The closer the stations are, the higher is the correlation between the signals. The reason is that in a short distance, the probability of the EPB not changing is greater. The middle panel in Figure 4 shows the temporal variation of the ionospheric delay processed by LTIAM for SAVO and SSA1 stations seen by the space vehicle 06 (PRN 06) for the day 001 of 2014 (1 January 2014) and the stations are 9,97 km apart each other. The same plasma bubble structures are clear in both stations, that is, a fast decreases in the ionospheric delays cross one station and after some time also cross the other. These features were used to develop our automatic criterions to identify and calculate the plasma bubble zonal velocity. The bottom panel in Figure 4 shows the satellite records for two stations far from each other. The stations are BELE (1°24'S, 48°27'W) and MABA (5°21'S, 49°7'W), and the distance between them are 443.20 km. The measurements of ionospheric delays are also for PRN 06 and occurred on 6 January 2013. It is remarkable that the structure of the irregularity changes greatly during the course of this distance, making it impossible to identify the same structure in the two sites using the pattern recognition algorithm. This is because when traveling long distances the plasma bubbles may present new bifurcations as well as dissipates those already existing and captured at the most distant GNSS receiving station. The bottom panel in Figure 4 is only one example in which data from stations separated by large distances cannot be used to calculate plasma bubble velocities according to the current method.

We have considered that plasma bubbles move in east-west direction, and the two stations chosen for this study are at the same magnetic latitude coincident with the direction of the bubble trajectory. Thence, our results are directly in magnetic coordinate.

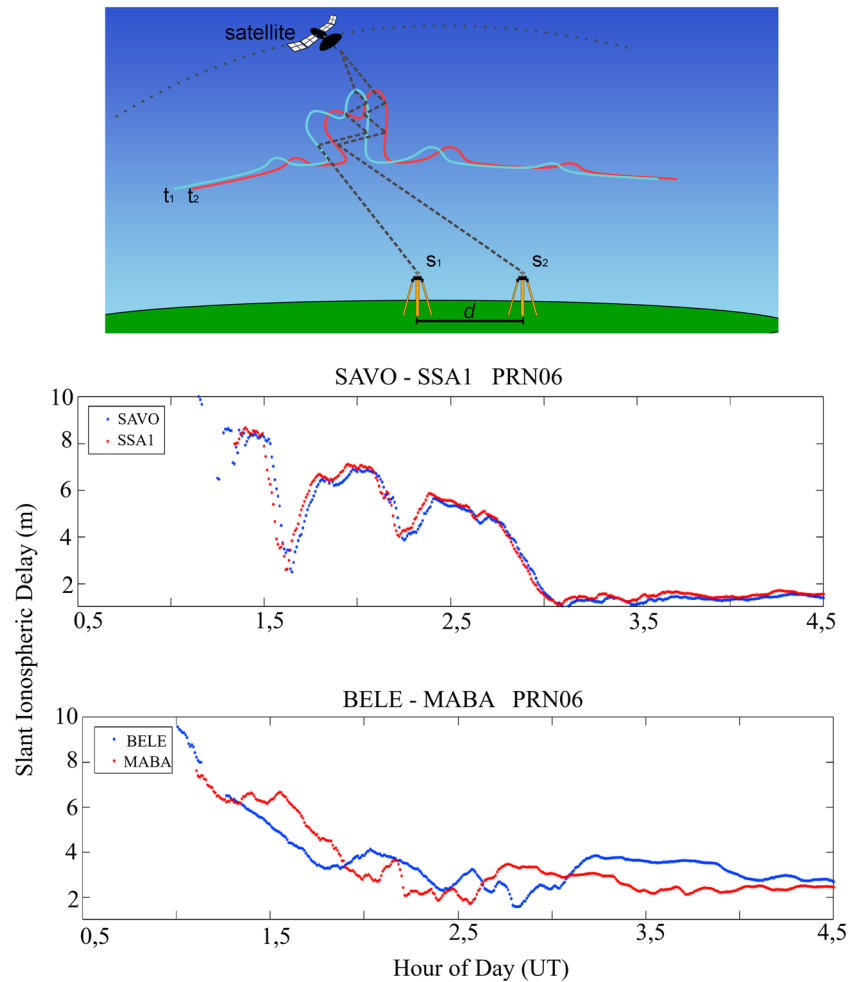


Figure 4. Top panel represents an illustration how about Two Station Method works. The equatorial plasma bubble is represented by the blue curve (in a first moment), then a red curve (second moment). The middle and bottom panels are Long-Term Ionospheric Anomaly Monitoring output plots representing the temporal variation of the ionospheric delay, when the stations are closer (middle panel) and far from (bottom panel) each other.

Since SAVO and SSA1 stations are very close to each other, the same irregularity structure is detected at each station, as discussed before. In order to ensure that each structure registered in a station is the same as the one registered in the adjacent station, it was used the *k*-means algorithm (Bang & Lee, 2013), a well-known pattern recognition algorithm.

K-means is a method of grouping data. This algorithm partitions *n* observations into *k* groups. Each observation belongs to the group closest to the mean. In other words, the *k*-means algorithm breaks the data into windows where each window has a portion of the two GNSS signals, one from each station, that exhibit similar behavior. Therefore, it is possible to assure that the corresponding structures registered at both stations are within the same analysis window. With the corresponding peaks marked in the same window, *k*-means saves the value of the abscissa corresponding to each peak and, from them, calculates the Δt . As the distance between the two GNSS receiver stations is known, it is possible to estimate the EPB velocities.

Besides to ensure the correct match between similar peaks, it is equally important to consider the velocity of the ionospheric pierce point (IPP), as it also moves. The IPP is defined as the intersection of the satellite line of sight and the ionospheric spherical shell. It is important to keep apart the IPP and EPB movements in order to calculate the EPB zonal drift velocities. The procedure to calculate the IPP velocities is given by Bang and Lee (2013). In addition, during the collection or processing of GNSS data, an elevation angle

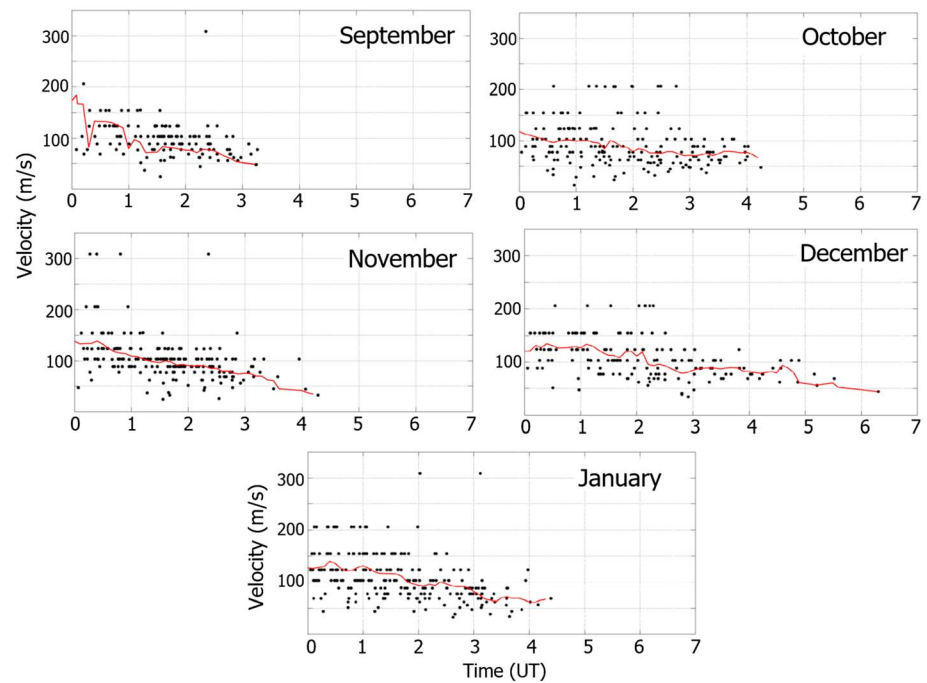


Figure 5. Equatorial plasma bubble zonal drift velocities calculated in this work. Each panel represents the set of all velocity values for each specific month. The red curve represents the moving average.

mask is often used to discard some observations. The purpose of this mask is to minimize high noise level data. The elevation mask used in this work is 40° .

To conclude, the EPB velocities calculated by LTIAM were compared with velocities calculated by keogram technique based on OI 630-nm airglow images. One of the advantages of the optical observation technique of EPBs is that each image is associated with an instant of time, making possible to estimate their velocities.

Each all-sky image provides an image with great optical distortion due to fisheye lens. To apply the keogram technique is necessary to linearize the images to then choose a line of pixels of each image, that is, a cut that crosses the whole image and that does not vary of position to each analyzed image. After that, the cuts are stacked into a single image forming the keogram.

3. Results and Discussion

In this section we will present and discuss the EPB zonal drift velocities calculated automatically using GNSS signals. To detect anomalous ionospheric behavior using GNSS signals is essential that the distance between one GNSS receiving station and another one does not exceed the 50 km, since this is established as a boundary condition under which the reliability of the method using the *k*-means algorithm is observed. This value was found after several tests, where we sought the highest efficiency and number of points returned by the algorithm. Stations very distant from each other may register the same structure into irregularity but present different satellite records because there is a possibility that the structure into irregularity may change during the course between one station and another. Thus, an analysis using very distant stations from each other would not be useful because it would hamper the pattern recognition necessary to assure that the stations were registering the same structure. Among other pairs of stations, the pair SAVO and SSA1 was chosen because they presented greater data coverage in detriment of other ones.

Figure 5 shows the overplots of the EPB zonal drift velocities calculated in this work. Each panel represents the set of all velocity values for each specific month; that is, each panel represents the junction of the velocity data calculated in this work for the specific month of study for the years 2012, 2013, and 2014. Thus, the top left panel refers to the set of all velocities obtained in this study for the months of September, the top right

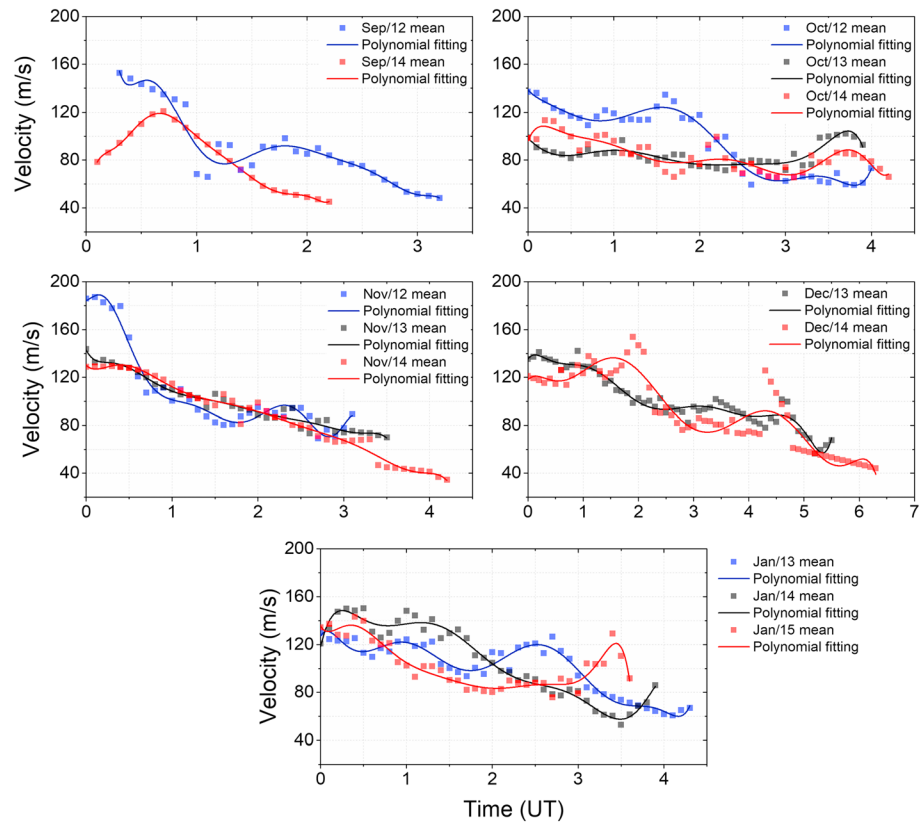


Figure 6. Mean (scatter) and polynomial fitting (curve) from equatorial plasma bubble velocities to each group of specific month.

panel for all months of October, and so on. Figure 5 also presents a moving average (red curve) in order to verify the average velocity behavior.

It is known cases which westward zonal motions have been observed, in spite of in less frequency (Sobral et al., 2011). However, all occurrences of EPBs studied in this work presented eastward movement; that is, no occurrence of westward plasma bubble movement was recorded. The confirmation of the eastward EPB movement was made by analyzing the OI 630-nm airglow images. This feature corroborates the methodology inserted in LTIAM.

A polynomial fitting applied to the average of each group of months is shown in Figure 6, where the average is represented by dots, while the polynomial fitting is shown by the solid curve. Similar to Figure 5, each panel represents a month. The adjustment that best represented the trend of velocities was the polynomial fit of ninth order. The present study examined EPB velocities during 24th solar cycle ascending phase taking into account the solar activity variation. It is interesting to note in December months the occurrence of a frequent characteristic of the zonal drift during the southern hemisphere summer for high solar activity, which is a sharp peak before dawn. These results are similar to those found by Fejer et al. (1991), with data from Jicamarca incoherent scatter radar. The occurrence of this characteristic in the LTIAM outputs makes it consistent with the study of the ionospheric behavior, since the irregularities seem to walk along with the movement of the ionospheric plasma.

Overall, Figure 6 presents great variability. Part of the variability presented when comparing the same month, for the different years of study, can be justified by the solar activity. Not only in relation to solar activity, the zonal velocities of the plasma bubbles also present variability according month of their occurrences and geomagnetic activity (Sobral et al., 2002; Terra et al., 2004). As the nocturnal velocities of zonal drift are consequences of the vertical electric fields generated by the *F* layer dynamo processes, which in turn are related to the neutral zonal winds, the more intense the neutral zonal winds are, the greater the electric fields, and consequently, the zonal drift velocities of the ionospheric bubbles are higher.

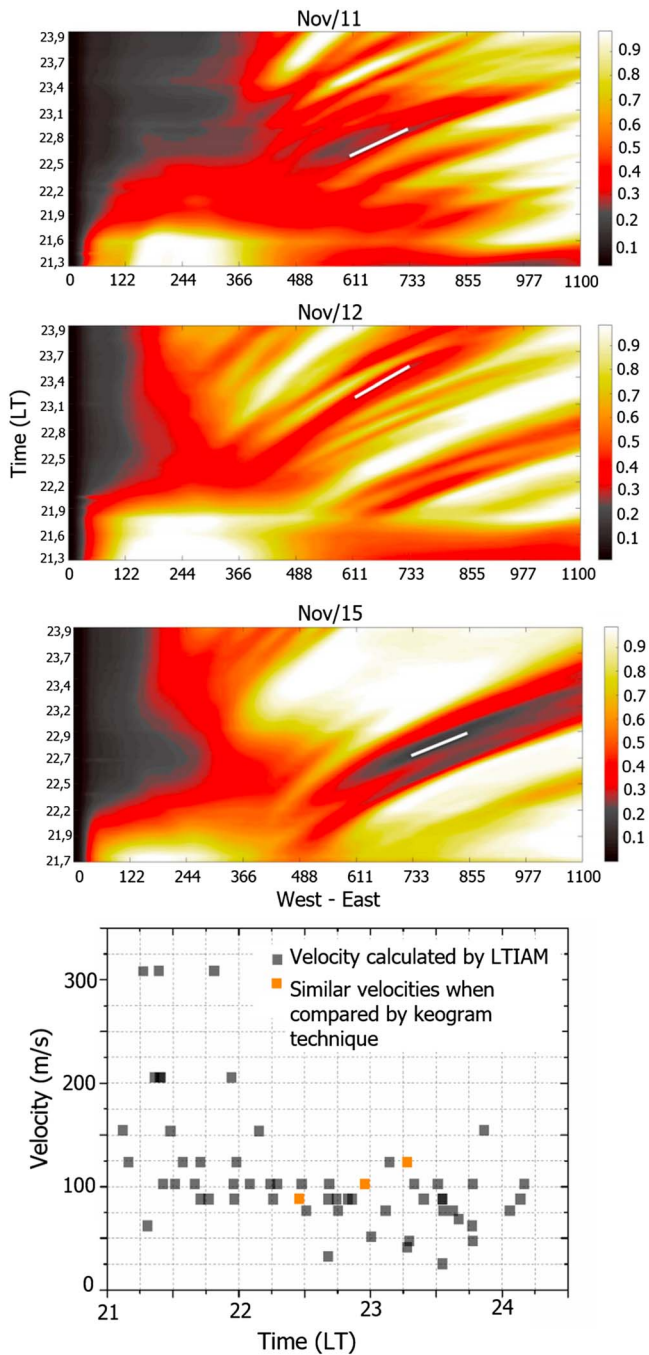


Figure 7. Keograms and scatter plot (bottom panel) from equatorial plasma bubble velocities comparing results from Long-Term Ionospheric Anomaly Monitoring and optical technique. The regions of equatorial plasma bubbles are represented by dark colors in keograms. The solid white line represents an interval that is possible to infer velocity value from coordinates of the final and start points. The orange squares in scatter plot represent similar velocities obtained by Long-Term Ionospheric Anomaly Monitoring in comparison to keogram technique.

A remarkable result of the present study regards the increase of the solar activity, marked by the peak years of the solar maximum, and the decrease of some velocities. These results were not expected and are different from finding by Fejer et al. (2005), where they found that near solar maximum, the zonal drifts have large magnitudes. Whereas, their analysis was based on radar observations, while our results are by satellite data. The direct relationship between solar activity and plasma bubble velocities is well known and has been noted in several research efforts (e.g., Sobral & Abdu, 1991; Fejer et al., 1991) among which they reinforce that higher values of F10.7 tend to raise the zonal velocity of the EPB. The hypothesis supported by the authors refers to the atypical form of the ascending phase of the Sun. The 24th solar cycle was double peaked with a long gap between them. After the first peak, occurred in 2012, the sunspot number decreases, just returning to recover and reaching the second peak in mid-2014 (solar maximum). In this work we consider 10 days as representative of each month; however, the ascending behavior of the solar activity during the gap between the peaks may have been influencing the unexpected low values of the EPB velocities in 2014 in comparison than 2012.

Moreover, in the recent study of Muella et al. (2017) they found that the generation of EPBs has been affected during solar cycle 24, since it was weaker in comparison to the previous cycle 23. In their analysis, the prevailing feature is the reduction in the EPB eastward velocities with the progression of the night, which is in agreement with the current work.

Regarding the period of observation of the EPBs, due to the limitation of the methodology implemented in LTIAM, the investigation of the plasma bubble through the RBMC network starts at 0000 UT (2100 LT). As plasma bubbles generally are formed in the post sunset period, it would be expected that at the beginning of our analysis period, the EPBs would already be present, as in fact they are seen in most of the panels presented in Figure 6. However, this did not occur in the months of September 2012 and 2014. It is known that the onset of these irregularities can be affected by disturbed electric field originated at high latitudes during magnetically disturbed conditions. However, during geomagnetically quiet conditions, as in the cases discussed in this paper, there are several processes such as neutral winds and conductivity of the *E* region that can inhibit the growth of irregularities or alter them. According to Sobral et al. (2002) September shows a lower probability of EPB occurrence than the other months (summer local). The bubbles observed at low latitude are the result of their upward growth at the geomagnetic equator and expansion along the flux tube, and consequently, it is expected a delay between the observation on the equator than on low latitudes. In addition, there are cases in which the bubbles do not reach altitudes at the equator high enough to be seen at low latitudes. This is one of the reasons why the occurrence of bubbles observed at low latitudes is lower when compared at the equator. Furthermore, Abdu et al. (2003) provided a statistical and empirical study which they pointed out that EPB occurrence has a strong seasonal dependence, which in equinoctial months the onset and peak occurrence of plasma bubbles are displaced to later hours at low latitudes. This justifies the late appearance of the plasma bubbles occurred in the September months of this study.

In order to compare, the EPB velocities calculated in this present work also were compared with velocities calculated by keogram technique based on all-sky OI 630-nm images. Three different days were used here

for the comparison of the velocities obtained by the LTIAM method and all-sky images. The keograms were formed from the cuts in all-sky linearized images for the nights of 11, 12, and 15 November 2012 obtained at the Brazilian northeastern station, Sao Joao do Cariri. Figure 7 shows three keograms and one scatter plot. In the keograms, the dark signatures describe the areas with the greatest rarefaction, that is, the regions of plasma bubbles. The color scale to the right of each panel represents the level of rarefaction in plasma density. It is possible to choose an interval between two points, where y axis represents the interval of time, while the x axis represents the zonal displacement of the structure. This interval between two points is represented in Figure 7 by a solid white line in keogram plots. As a result, the velocity may be calculated. Taking into account the coordinates of the initial and final points, the velocities estimated were 87.05, 97, and 135.8 m/s for each panel, respectively, from the top to the third panel. The bottom panel in Figure 7 shows the comparison between these velocities obtained with our method and by the keogram technique. All velocities in bottom panel were calculated using GNSS signals, as explained in this work; however, the orange squares represent the velocities similar to the values obtained in the keograms. As we can see, our values are coherent with the one obtained by comparison to a well-known optical methodology.

4. Summary and Conclusions

In this paper the LTIAM was used to monitor the plasma bubbles, allowing to automatically infer EPB zonal drift velocities from two GNSS receiving stations close to each other, for geomagnetically quiet periods.

The LTIAM code was modified to perceive the passage of the ionospheric irregularity between two stations of the RBMC network. However, for large distances from each other, the reliability of the methodology is reduced. As soon as both stations record the irregularity, the k -means algorithm checks the time interval during the passage of the irregularity in each station, to then provide the velocity value.

The velocities calculated by LTIAM presented considerable variability, which was already expected. By analyzing the velocities obtained, LTIAM provided all velocities with positive values (convention: positive values represent propagation to eastward). After inspection of images in the emission of the OI 630 nm, it was verified that all the occurrences of plasma bubbles presented movement toward the east. That is, within the database there was no bubble westward velocity. This fact corroborates the reliability of the method. The LTIAM was also able to reproduce a characteristic of ionospheric plasma, similar to that already announced by Fejer et al. (1991), which refers to a peak in zonal drift during the summer for high solar activity. This similarity is quite consistent with the behavior of ionospheric plasma, since the irregularities seem to move along with the movement of the plasma.

The average results obtained using LTIAM are in accordance with the values published in the literature. They were larger at the start time of the analysis (2100LT), reaching values of 300 m/s in a timely but occasional way, that is, higher velocities at the start time of the analysis and subsequent decay in the late night hours. This trend is attributed to the dynamics of the neutral winds, since they have lower intensity in the late evening and early in the day.

By fixing a month and analyzing the variations in mean velocities results for the different years of study, it was expected to verify the influence of solar activity. Since the higher the solar flux, the higher the EPB zonal velocities. However, even with the increase in F10.7, there was a decrease in some velocities values. The hypothesis supported by the authors refers to the atypical double peaked 24th solar cycle form, where the first peak was considered ascending phase, while the second peak was considered the solar maximum. As a result, the trend of F10.7 was to decrease between peaks, even though the years of study are presented as the growth of solar activity going from the ascending phase to the solar maximum. Still in the monthly analysis, September months present late occurrence of plasma bubbles. This is attributed to the strong seasonal dependence of EPBs.

To conclude, the EPB velocities calculated by LTIAM were also compared with velocities calculated by keogram technique based on all-sky OI 630-nm images. There were no significant differences between the speeds calculated by the LTIAM technique and keogram, since the results were fully compliant with the airglow technique.

Acknowledgments

R. P. Silva acknowledges the support from Conselho Nacional de Desenvolvimento Científico e Tecnológico (CNPq). This work was supported in part by grants 140788/2015-8 and 300813/2018-0. J. R. De Souza would like to thank CNPq (305885/2015-4) and also INCT GNSS-NavAer supported by CNPq (465648/2014-2), FAPESP (2017/50115-0), and CAPES (88887.137186/2017-00). J. H. A. Sobral thanks CNPq for grant 303741/2014-7. C. M. Denardini thanks CNPq/MCTIC (grant 303643/2017-0) and FAPESP (grant 2012/08445-9), and G. L. Borba thanks AEB (grant PIB10467-2013). We are grateful to Cristiano Wrasse, INPE, for providing the OI 630-nm airglow images treated, and with the stars removed. We also would like to thank J. Sousasantos whose scientific discussions were particularly helpful. The authors acknowledge Richard Cole from Mirus Technology, LLC, for the permission to use the LTIAM code, which was developed by Korea Advanced Institute of Science and Technology, and RBMC network for making data available (<https://ww2.ibge.gov.br/home/geociencias/geodesia/rbmc/rbmc.shtm?c=7>).

References

- Aarons, J. (1993). The longitudinal morphology of equatorial *F*-layer irregularities relevant to their occurrence. *Space Science Reviews*, 63(3-4), 209–243. <https://doi.org/10.1007/BF00750769>
- Abdu, M. A. (2001). Outstanding problems in the equatorial ionosphere–thermosphere electrodynamics relevant to spread *F*. *Journal of Atmospheric and Solar-Terrestrial Physics*, 63(9), 869–884. [https://doi.org/10.1016/S1364-6826\(00\)00201-7](https://doi.org/10.1016/S1364-6826(00)00201-7)
- Abdu, M. A., Medeiros, R. T., Sobral, J. H. A., & Bittencourt, J. A. (1983). Spread *F* plasma bubble vertical rise velocities determined from spaced ionosonde observations. *Journal of Geophysical Research*, 88(A11), 9197–9204. <https://doi.org/10.1029/JA088A11p09197>
- Abdu, M. A., Muralikrishna, P., Batista, I. S., & Sobral, J. H. A. (1991). Rocket observation of equatorial plasma bubbles over Natal, Brazil, using a high-frequency capacitance probe. *Journal of Geophysical Research*, 96(A5), 7689–7695. <https://doi.org/10.1029/90JA02384>
- Abdu, M. A., Souza, J. R., Batista, I. S., & Sobral, J. H. A. (2003). Equatorial spread *F* statistics and empirical representation for IRI: A regional model for the Brazilian longitude sector. *Advances in Space Research*, 31(3), 703–716. [https://doi.org/10.1016/S0273-1177\(03\)00031-0](https://doi.org/10.1016/S0273-1177(03)00031-0)
- Bang, E., & Lee, J. (2013). Methodology of automated ionosphere front velocity estimation for ground-based augmentation of GNSS. *Radio Science*, 48, 659–670. <https://doi.org/10.1002/rds.20066>
- Burke, W. J., Gentile, L. C., Huang, C. Y., Valladares, C. E., & Su, S. Y. (2004). Longitudinal variability of equatorial plasma bubbles observed by DMSP and ROCSAT-1. *Journal of Geophysical Research*, 109, A12301. <https://doi.org/10.1029/2004JA010583>
- Datta-Barua, S., Lee, J., Pullen, S., Luo, M., Ene, A., Qiu, D., et al. (2010). Ionospheric threat parameterization for local area global-positioning-system-based aircraft landing systems. *Journal of Aircraft*, 47(4), 1141–1151. <https://doi.org/10.2514/1.46719>
- de Rezende, L. F. C., de Paula, E. R., Kantor, I. J., & Kintner, P. M. (2007). Mapping and survey of plasma bubbles over Brazilian territory. *The Journal of Navigation*, 60(1), 69–81. <https://doi.org/10.1017/S0373463307004006>
- Fejer, B. G., Paula, E. D., Gonzalez, S. A., & Woodman, R. F. (1991). Average vertical and zonal *F* region plasma drifts over Jicamarca. *Journal of Geophysical Research*, 96(A8), 13,901–13,906. <https://doi.org/10.1029/91JA01171>
- Fejer, B. G., Souza, J. R., Santos, A. S., & Costa Pereira, A. E. (2005). Climatology of *F* region zonal plasma drifts over Jicamarca. *Journal of Geophysical Research*, 110, A12310. <https://doi.org/10.1029/2005JA011324>
- Haase, J. S., Dautermann, T., Taylor, M. J., Chapagain, N., Calais, E., & Pautet, D. (2011). Propagation of plasma bubbles observed in Brazil from GPS and airglow data. *Advances in Space Research*, 47(10), 1758–1776. <https://doi.org/10.1016/j.asr.2010.09.025>
- Haerendel, G., Eccles, J. V., & Cakir, S. (1992). Theory for modeling the equatorial evening ionosphere and the origin of the shear in the horizontal plasma flow. *Journal of Geophysical Research*, 97(A2), 1209–1223. <https://doi.org/10.1029/91JA02226>
- Huang, C. S., & Kelley, M. C. (1996). Nonlinear evolution of equatorial spread *F*: 4. Gravity waves, velocity shear, and day-to-day variability. *Journal of Geophysical Research*, 101(A11), 24,521–24,532. <https://doi.org/10.1029/96JA02332>
- Huang, C. Y., Burke, W. J., Machuzak, J. S., Gentile, L. C., & Sultan, P. J. (2002). Equatorial plasma bubbles observed by DMSP satellites during a full solar cycle: Toward a global climatology. *Journal of Geophysical Research*, 107(A12), 1434. <https://doi.org/10.1029/2002JA009452>
- Huba, J. D., & Joyce, G. (2010). Global modeling of equatorial plasma bubbles. *Geophysical Research Letters*, 37, L17104. <https://doi.org/10.1029/2010GL044281>
- Jung, S., & Lee, J. (2012). Long-term ionospheric anomaly monitoring for ground based augmentation systems. *Radio Science*, 47, RS4006. <https://doi.org/10.1029/2012RS005016>
- Kelley, M. C. (2009). *The Earth's Ionosphere: Plasma Physics and Electrodynamics*, (Vol. 96). London: Academic Press.
- LaBelle, J., Jahn, J. M., Pfaff, R. F., Swartz, W. E., Sobral, J. H. A., Abdu, M. A., et al. (1997). The Brazil/Guará equatorial spread *F* campaign: Results of the large scale measurements. *Geophysical Research Letters*, 24(13), 1691–1694. <https://doi.org/10.1029/97GL00818>
- Lee, J., Datta-Barua, S., Zhang, G., Pullen, S., & Enge, P. (2011). Observations of low-elevation ionospheric anomalies for ground-based augmentation of GNSS. *Radio Science*, 46, RS6005. <https://doi.org/10.1029/2011RS004776>
- Moraes, A. D. O., Vani, B. C., Costa, E., Abdu, M. A., de Paula, E. R., Sousasantos, J., et al. (2018). GPS availability and positioning issues when the signal paths are aligned with ionospheric plasma bubbles. *GPS Solutions*, 22(4), 95. <https://doi.org/10.1007/s10291-018-0760-8>
- Muella, M. T., Duarte-Silva, M. H., Moraes, A. O., de Paula, E. R., de Rezende, L. F., Alfonsi, L., & Affonso, B. J. (2017). Climatology and modeling of ionospheric scintillations and irregularity zonal drifts at the equatorial anomaly crest region. *Annales de Geophysique*, 35(6), 1201–1218. <https://doi.org/10.5194/angeo-35-1201-2017>
- Pullen, S., Park, Y. S., & Enge, P. (2009). Impact and mitigation of ionospheric anomalies on ground-based augmentation of GNSS. *Radio Science*, 44, RS0A21. <https://doi.org/10.1029/2008RS004084>
- Sobral, J. H., de Castilho, V. M., Abdu, M. A., Takahashi, H., Paulino, I., Gasparelo, U. A., et al. (2011). Midnight reversal of ionospheric plasma bubble eastward velocity to westward velocity during geomagnetically quiettime: Climatology and its model validation. *Journal of Atmospheric and Solar-Terrestrial Physics*, 73(11-12), 1520–1528. <https://doi.org/10.1016/j.jastp.2010.11.031>
- Sobral, J. H. A., & Abdu, M. A. (1991). Solar activity effects on equatorial plasma bubble zonal velocity and its latitude gradient as measured by airglow scanning photometers. *Journal of Atmospheric and Terrestrial Physics*, 53(8), 729–742. [https://doi.org/10.1016/0021-9169\(91\)90124-P](https://doi.org/10.1016/0021-9169(91)90124-P)
- Sobral, J. H. A., Abdu, M. A., & Batista, I. S. (1980). Airglow studies on the ionosphere dynamics over low latitude in Brazil. In *Annales de Geophysique* (Vol. 36, pp. 199–204). São José dos Campos: INPE.
- Sobral, J. H. A., Abdu, M. A., Takahashi, H., Taylor, M. J., de Paula, E. R., Zamlutti, C. J., et al. (2002). Ionospheric plasma bubble climatology over Brazil based on 22 years (1977–1998) of 630 nm airglow observations. *Journal of Atmospheric and Terrestrial Physics*, 64(12), 1517–1524. [https://doi.org/10.1016/S1364-6826\(02\)00089-5](https://doi.org/10.1016/S1364-6826(02)00089-5)
- Sobral, J. H. A., Abdu, M. A., Zamlutti, C. J., & Batista, I. S. (1980). Association between plasma bubble irregularities and airglow disturbances over Brazilian low latitudes. *Geophysical Research Letters*, 7(11), 980–982. <https://doi.org/10.1029/GL007i011p00980>
- Sousasantos, J., Kherani, E. A., & Sobral, J. H. A. (2017). An alternative possibility to equatorial plasma bubble forecasting through mathematical modeling and Digisonde data. *Journal of Geophysical Research: Space Physics*, 122, 2079–2088. <https://doi.org/10.1002/2016JA023241>
- Takeyasu, S., Keisuke, M., Takayuki, Y., & Susumu, S. (2009). Air navigation with global navigation satellite systems and the ionospheric effects. *Journal of the National Institute of Information and Communications Technology*, 56(1-4), 231–242.
- Terra, P. M., Sobral, J. H. A., Abdu, M. A., Souza, J. R., & Takahashi, H. (2004). Plasma bubble zonal velocity variations with solar activity in the Brazilian region. *Annales Geophysicae*, 22(9), 3123–3128. <https://doi.org/10.5194/angeo-22-3123-2004>